Small Crack Growth Path and Rate under Combined Stresses

N. Shamsaei[1] and A. Fatemi[2]

[1]Durability Engineer, Chrysler Group LLC
Chelsea Proving Grounds, 3700 South M-52, Chelsea, MI 48118, USA
ns745@chrysler.com, Fax: 734-475-5565

[2]Professor, Mechanical, Industrial and Manufacturing Engineering,
The University of Toledo, 2801 West Bancroft Street, Toledo, OH 43606, USA
afatemi@eng.utoledo.edu, Fax: 419-530-8213

ABSTRACT. *A significant portion of the fatigue life is typically spent in growth of small cracks. In addition, the stress state in many structures and components is multiaxial. Therefore, the study of small crack growth behavior with regards to its growth path as well as growth rate under combined stresses can be of great importance in many applications. This study investigates small crack growth behavior of several steels under multiaxial states of stress. Experimental observations from solid and thin-walled tubular round specimens under various multiaxial cyclic loadings including in-phase and out-of-phase, tension-torsion and tension-tension, and with or without mean stresses are used to characterize small crack growth behavior. The steels used include 1045 and 1050 medium carbon steels, 304L stainless steel, and Inconel 718. Effects of load non-proportionality, mean stresses, and friction-induced closure on small fatigue crack growth behavior are discussed. Critical plane analysis and an effective strain intensity factor are used to predict crack growth path as well as to correlate crack growth rates under various combined stress conditions.*

Keywords: Small crack growth path; Small crack growth rate; Multiaxial loading; Combined stresses, Non-proportional loading; Mean stress effects

INTRODUCTION

Stress and strain states of many industrial components and structures are multiaxial, which arises from multi-directional loading, residual stresses, or geometrical effects. Fatemi and Shamsaei [1] have recently reviewed some of the most important issues to be considered in multiaxial fatigue analysis and life estimation. One issue among these is crack growth under combined stresses, as it can constitute a significant portion of the total fatigue life.

The fatigue process includes initiation and growth of micro-cracks. Crack initiation life consists of crack nucleation and micro-crack growth up to a length of typically about several hundred micrometer (i.e. microscopic growth), as presented in Fig. 1. At

this length scale, microstructure texture and crack surface morphology can play a dominant role on crack growth behavior. The crack growth life typically consists of a period of small crack growth followed by long crack growth (i.e. macroscopic growth). For the small crack growth regime, the crack is typically affected by the local plasticity and does not generate its own plastic zone. In contrast, longer cracks at the macroscopic level are generally less affected by the local plasticity and they generate their own plastic zone at the crack tip. Modeling of such cracks typically requires the use of fracture mechanics analysis.

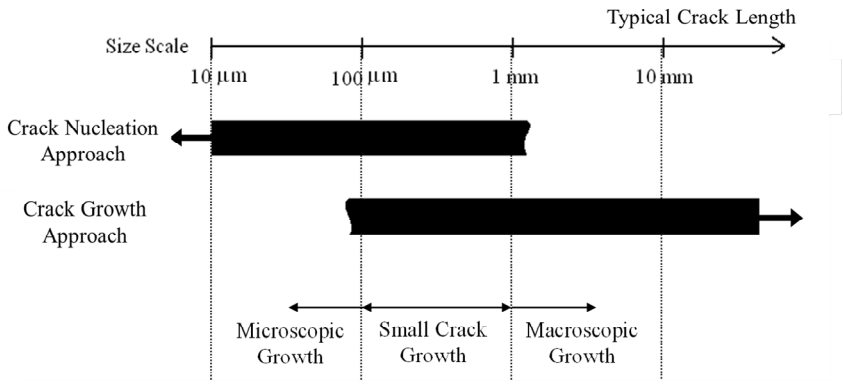

Figure 1. Different stages of crack nucleation and growth during the fatigue process and the approach typically used for analysis.

Experimental observations suggest material, load magnitude, initial crack tip condition, load ratio, and mean stress affect the crack growth mode [2]. In plate-type geometries, although cracks may form under mixed-mode loading, they often turn into a mode I macro-crack soon after micro-crack growth. Thin-walled tubular specimens under torsion loading can be used to generate mode II macro-crack growth. Mixed-mode fatigue crack growth behavior may be affected by different factors such as overloads, crack closure, T-stress, and load non-proportionality.

Since the crack changes direction during its growth under mixed-mode loading, both crack growth rate and crack growth direction need to be considered [2-4]. Several criteria for prediction of crack growth direction under mixed-mode loadings have been proposed over the last 50 years. Among these, the maximum tangential stress (MTS) [5] and the minimum strain energy density [6] criteria are most commonly used due to their simplicity as well as support by experimental observations [7, 8]. The MTS criterion considers the direction of crack growth to correspond with the maximum tangential stress direction. The minimum strain energy density criterion predicts crack growth to be in a direction along which the strain energy density reaches its minimum. However, applications of these criteria are generally limited to the linear elastic fracture mechanics regime.

To correlate fatigue crack growth rates under mixed-mode loading, effective strain and effective stress intensity factors have been used. Crack growth life can then be calculated by integrating a Paris-type equation. Effective stress intensity factors include

one proposed by Tanaka [9] and effective strain intensity factors include those proposed by Socie et al. [10] and by Reddy and Fatemi [11]. The effective stress-based intensity factor proposed by Tanaka [9] assumes fatigue crack growth occurs when the sum of the absolute values of the crack tip displacements in a plastic strip reaches a critical value. The effective strain-based intensity factor proposed by Reddy and Fatemi [11] is based on the Fatemi-Socie critical plane fatigue damage parameter, given by:

$$\Delta K_{CPA} = G\,\Delta\gamma_{\max}\left(1+k\frac{\sigma_{n,\max}}{\sigma_y}\right)\sqrt{\pi\,c} \qquad (1)$$

Hoshide and Socie [12] also extended the J-integral concept, originally proposed for correlation of crack growth rate under mode I, to mixed-mode crack growth.

This study investigates small crack growth behavior of 1045 and 1050 medium carbon steels, 304L stainless steel, and Inconel 718 under multiaxial states of stress. Experimental observations from solid and thin-walled tubular round specimens under various combined stresses including in-phase and out-of-phase, tension-torsion and tension-tension, and with or without mean stresses are used to characterize small crack growth behavior. Effects of friction-induced closure, material ductility, stress gradient, strain amplitude, non-proportionality of loading, and mean stress on small fatigue crack growth behavior are discussed. The Reddy-Fatemi critical plane effective strain-based intensity factor is then used to correlate crack growth rate data for various materials and loading conditions presented.

EXPERIMENTAL DATA AND OBSERVATIONS

Materials and Loading Conditions

Tubular specimens with a gage section wall thickness of 1.25 mm were made of 1050 medium carbon steel in normalized condition (N) with Brinell hardness (HB) of 198 and pearlitic-ferritic microstructure and in quenched and tempered (QT) condition and HB of 360 and tempered martensite microstructure were used. Tubular specimens were also made of 304L stainless steel with austenitic microstructure. Details of specimen dimensions and testing procedure can be found in [13]. In addition, some 1050 normalized steel solid specimens were also machined to the same outer configuration and dimensions of normalized tubular specimens with no hole to study the effect of stress gradient on crack growth behavior. The inside of the tubular specimens were honed and three different grits of aluminum oxide films were used for both solid and tubular specimens to provide a near to mirror outer surface finish in the gage section of all specimens.

A closed-loop servo-controlled hydraulic axial-torsion load frame was used to conduct the tests. Cellulose acetate sheet replication method was employed to monitor specimen surface crack growth. Wherever applicable, tests were performed according to ASTM Standard E2207 [14]. Details of the experimental procedure, fatigue behavior,

and material properties for 1050 N and 1050 QT steels as well as 304L stainless steel can be found in [13, 15]. In addition to the 1050 steel data in N and QT conditions and 304L stainless steel crack growth data generated for this study, tubular specimen crack growth data for 1045 steel in normalized (N) condition and for Inconel 718 data under various loading paths as summarized in [11] were also utilized.

The loading paths analyzed are presented in Fig. 2. Strain paths B, K, and L represent torsion (shear) cycles with no mean, with tensile normal mean stress/strain, and with compressive normal mean stress/strain, respectively. These paths were used to study the effect of closure on crack growth behavior. Strain paths C for in-phase (IP) and N for 90º out-of-phase (OP) loading were used to investigate effects of load non-proportionality on crack growth behavior. Effects of axial and/or torsion mean stresses on crack growth were studied employing strain paths E, F, G, H, J, and O. Crack growth behavior under biaxial tension-tension loading was investigated by using load paths, U, V, and W.

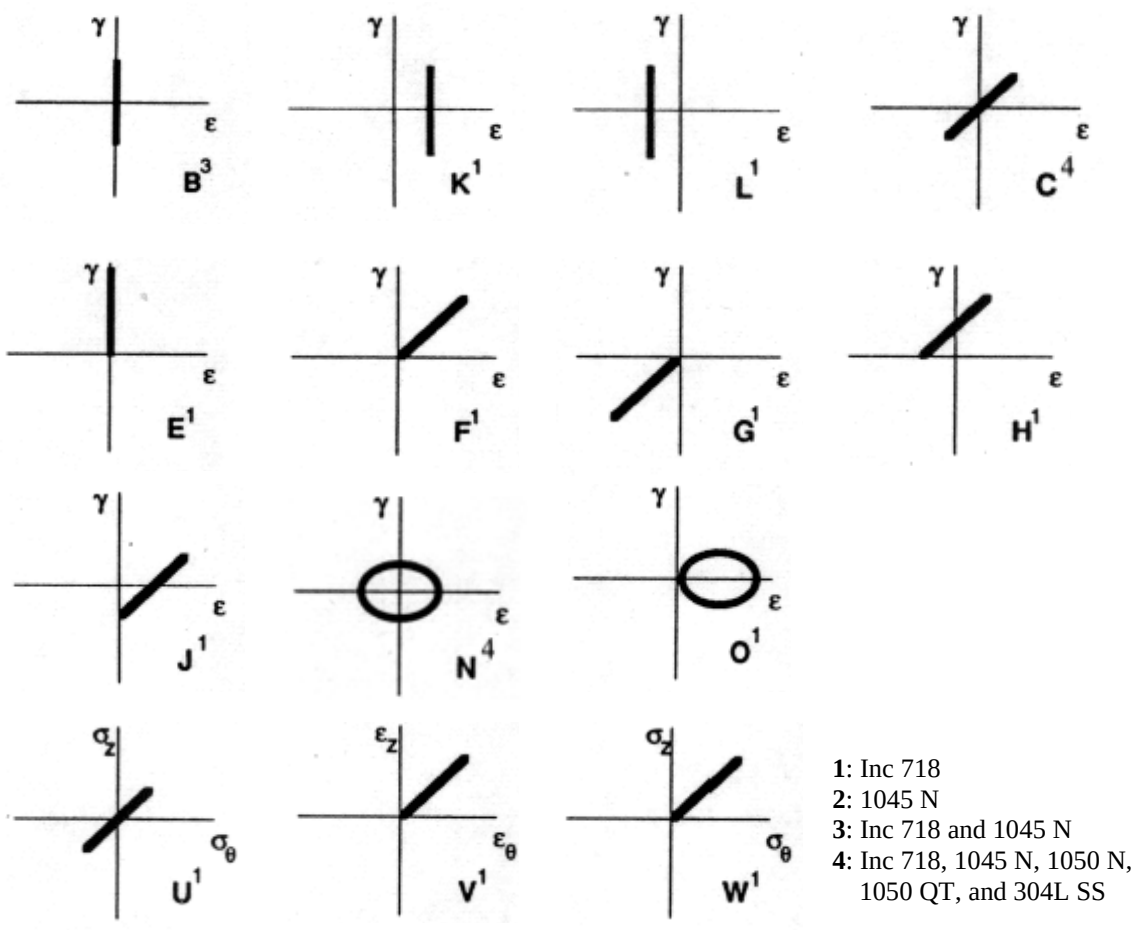

Figure 2. Load paths used to study various effects on crack growth behavior [11]. The superscript on each path code identifies the material(s) for which the load path was used.

Overall Cracking Behavior

Beer [16] reported a semi-elliptical curve could well represent crack profiles of specimens under axial, torsion, and axial-torsion loading. A good correlation between crack depth and surface crack length was also reported for crack lengths between the range of 100 μm and 2 mm. Therefore, surface crack length was used as an indicator of crack depth and geometry in this study.

Cracks for all loading conditions were found to be on or about the maximum shear plane for 1050 N, 1050 QT, and 304L steels in this study, as well as for 1045 N steel and Inconel 718 as reported in [11, 17]. Figure 3 presents examples of cracks observed for IP and OP loadings with low and high strain amplitudes for 1050 N steel. In most cases, particularly for 1050 N steel and 304L stainless steel and in tests with high strain amplitude, several cracks were observed. However, one crack became dominant and grew to be the failure crack. Longer cracks were observed on the planes oriented on a narrower range, whereas shorter cracks appeared to be on a wider range of planes around the critical plane. Microstructural features such as grain shape, size, and

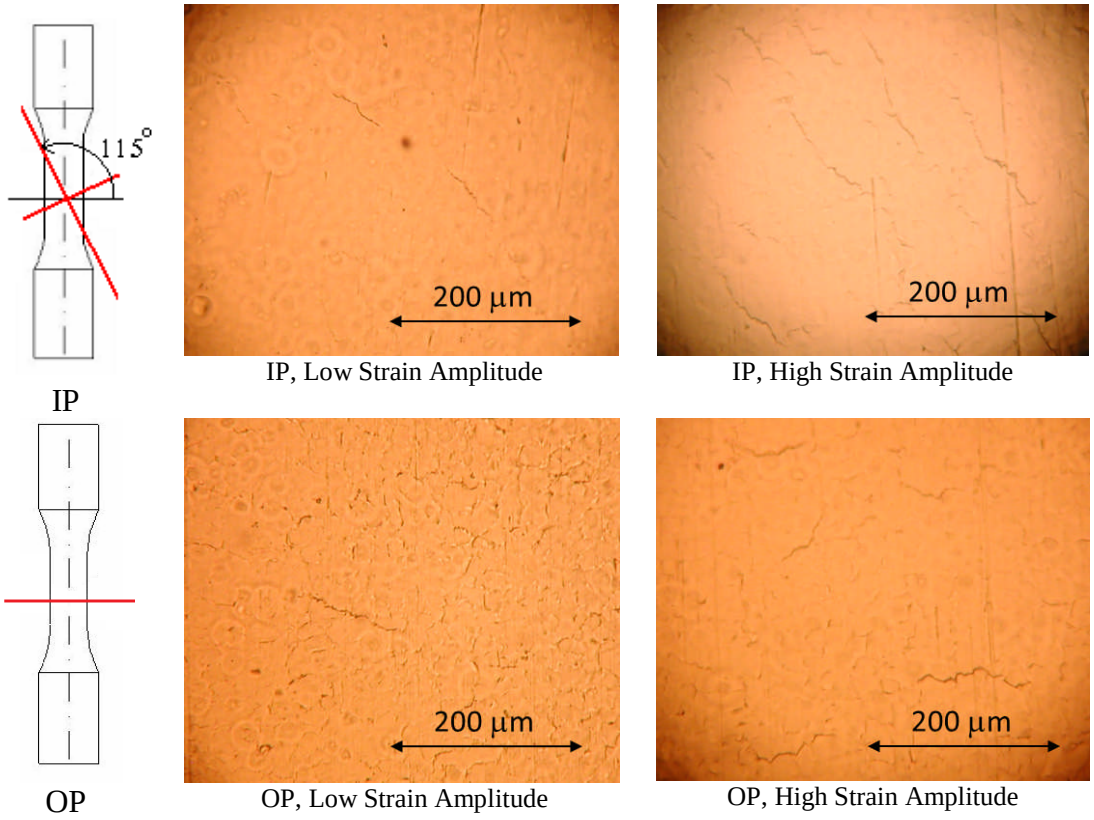

Figure 3. Cracks observed under in-phase (IP) and 90º out-of-phase (OP) loading for low and high strain amplitude tests of 1050 N steel specimens. Critical planes for IP (115º) and OP (0º) loadings are also shown.

orientation affect the micro-cracks behavior, whereas longer cracks grow under control of the shear driving force and independent of such features. Coalescence of cracks sometimes caused a sudden increase in crack length. Crack shielding was also often observed to stop or retard the growth of a small crack which was parallel to a long crack. More details regarding these observations including number and range of observed cracks as well as additional crack photos can be found in [18].

As can be seen from Fig. 3, shear cracks typically have a zigzag pattern. Thus, crack surface roughness can result in friction induced closure. Figure 4(a) compares crack length versus number of cycles for Inconel 718 under cyclic shear strain with tensile (path K) and with compressive (path L) mean normal stress/strain. Compressive normal stress/strain on maximum shear plane for load path L closes the crack, decelerates crack growth process and extends fatigue life, whereas tensile normal stress/strain for load path K opens the crack, accelerates crack growth process and shortens fatigue life. Additional examples of friction induced closure and differences in crack growth rates and fatigue lives between paths K and L in high cycle fatigue are presented in [11, 17].

Effects of Material Ductility and Stress Gradient

More cracks were observed for more ductile behaving materials such as 304L stainless steel and 1050 N steel, as compared to the more brittle behaving 1050 QT steel. A comparison of micro-crack growth for IP tests (path C) of tubular specimens for 1050 N steel and 1050 QT steel is shown in Fig. 4(b). Shorter cracks were detected at earlier stage of fatigue life for 1050 N steel, as compared to 1050 QT steel. As can be seen from this figure, crack growth rate is also higher for 1050 QT steel as compared to 1050 N steel.

Many more cracks in various sizes were observed for solid specimens as compared to the tubular specimens of 1050 N steel. A comparison of micro-crack growth for IP tests (path C) of solid and tubular specimens of 1050 N steel is made in Fig. 4(c). Cracks nucleated at smaller percentage of fatigue life for the solid specimen as compared to the tubular specimen. As can be observed from this figure, crack growth rate was higher for tubular specimens as compared to solid specimens, which explains the presence of more cracks for solid specimens. This also explains longer fatigue lives observed for the solid specimens [13]. Lower crack growth rate observed for solid specimens can result from the gradient of shear stress in the solid section, while shear stress is nearly uniform in the thin-walled tubular section.

Effects of Strain Amplitude

More cracks were observed for higher amplitude tests, as compared to lower amplitude tests for both in-phase (IP) and 90° out-of-phase (OP) loadings, as can be seen from Fig. 3 for 1050 N steel. Cracks were also observed on a wider range of plane orientations for higher strain amplitude level tests of both IP and OP loadings. This can be explained by the fact that the damage value on planes near the critical plane is a high

percentage of the critical plane damage value. As cracks in shear failure mode materials are a consequence of active slip systems, shear stress and the number of applied cycles should reach a critical level to activate slip systems on a specific plane. Higher amplitude loading results in exceeding of the shear stress on a wider range of planes around the maximum shear or damage plane and, therefore, slip systems are activated on more planes. As a result, cracks are nucleated on a wider range of planes for higher amplitude level tests. More details regarding these observations can be found in [18].

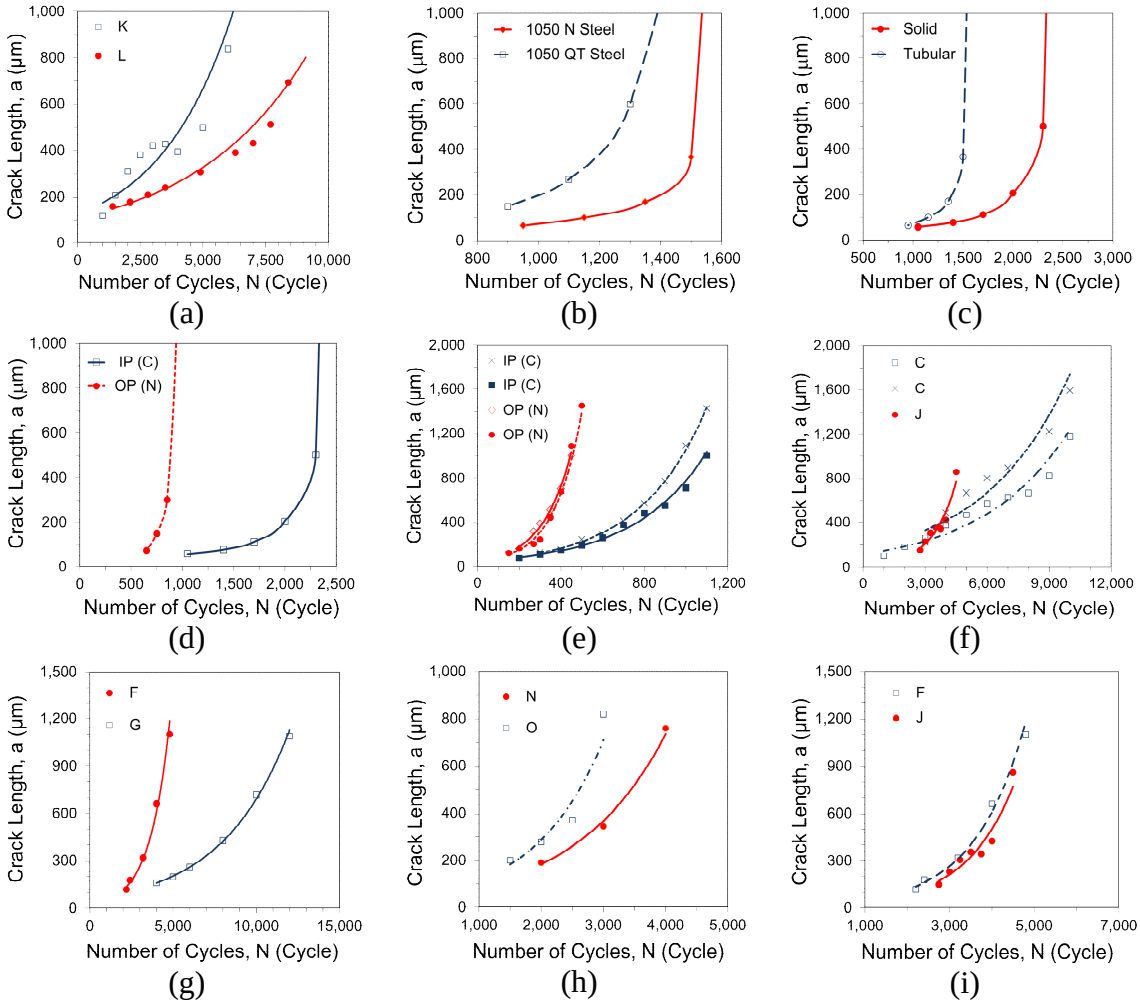

Figure 4. (a) Crack length versus number of cycles under cyclic shear with tensile (path K) and compressive (path L) mean normal stress for Inconel 718. (b) Effect of material ductility on cracking behavior under IP loading (path C). (c) Stress gradient effect on cracking behavior under IP loading for 1050 N steel. Effect of load non-proportionality on crack growth behavior of 1050 N steel solid specimens (d) and Inconel 718 (e). Effect of mean tensile stress on crack growth behavior under IP loading (f and g) and OP loading (h) of Inconel 718. (i) Effect of mean shear stress on crack growth behavior of Inconel 718.

Mechanism of micro-crack evolution for high and intermediate amplitude strain level tests of 1050 N steel was observed to be a combination of crack growth and coalescence of multiple cracks, whereas the evolution mechanism for low amplitude tests was found to be crack growth of a single dominant crack. Crack nucleation was also observed to occur at a much earlier stage of fatigue life for high strain amplitude tests, as compared to lower amplitude fatigue tests. As expected, crack growth rate was also found to be higher for the higher amplitude level tests.

Effects of Load Non-proportionality

More cracks were observed for in-phase (IP) loading (path C) as compared to 90º out-of-phase (OP) loading (path N) at the same strain level, as presented in Fig. 3 for 1050 N steel. Crack lengths versus number of cycles are superimposed for IP and OP tests of this material in Fig. 4(d). As can be seen from this figure, the crack growth rate is higher for OP loading as compared to IP loading. A similar behavior was also reported for Inconel 718 [11], as shown in Fig. 4(e). A higher normal stress on the maximum shear plane for OP loading as compared to IP loading can explain the observed higher crack growth rate in OP loading. This is even true for materials without non-proportional cyclic hardening, such as 1050 QT steel [15] and Titanium [19].

Variations of maximum shear strain amplitude and maximum normal stress for 304L stainless steel under IP (path C) and OP (path N) loading are presented in Fig. 5. It can be seen from this figure that the maximum shear strain amplitude and maximum normal stress components reach their maximum values on the 0º plane (i.e. critical plane) for the OP example, therefore, the maximum shear and maximum principal planes are the same. The higher tensile normal stress on the maximum shear plane for OP loading opens the crack and increases the crack growth rate, as compared to IP loading. The *FS* parameter represents this observation, resulting in higher damage value for OP loading and, therefore, shorter fatigue life prediction. As mentioned earlier, this behavior is also true for materials without non-proportional cyclic hardening, as discussed in [1].

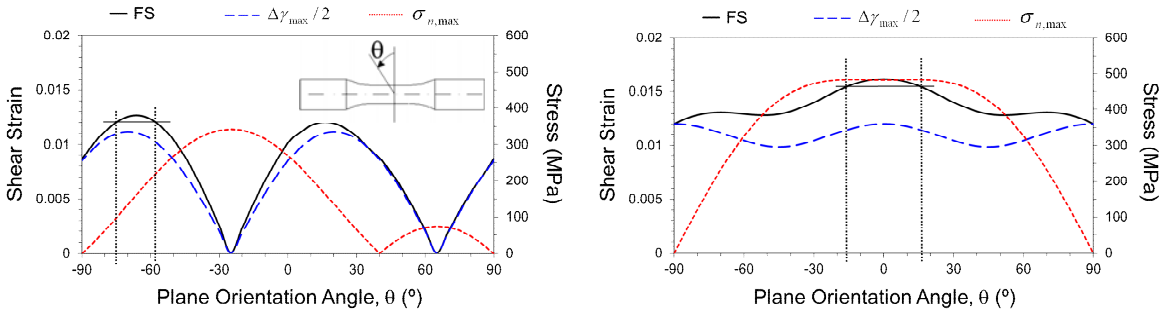

Figure 5. Variation of maximum shear strain amplitude, maximum normal stress, and *FS* damage parameter for 304L stainless steel at equivalent strain amplitude of $\bar{\varepsilon}_a = 0.007$ under (a) IP (path C), and (b) OP (path N) loading.

Micro-cracks were also observed over a wider range of plane orientations for OP loading, as compared to IP loading. Presence of cracks on a wider range of planes around the critical plane for OP loading can be explained by a wider distribution of damage, where planes around the critical plane experience a high percentage of damage value. The range of planes experiencing 95% of the maximum damage are shown in Fig. 5 for IP loading as ±9º, while for OP loading this range is ±17º. The difference in crack orientation range observed for IP and OP loadings decreases by a decrease in strain amplitude level. More details regarding these observations can be found in [18].

Effects of Mean Stress

As presented in Fig. 4(a) for a simple shear cyclic loading path, a compressive normal stress/strain on the maximum shear plane decelerates crack growth and extends fatigue life, whereas a tensile normal stress/strain accelerates crack growth and shortens fatigue life. Similar effects of normal mean stress/strain on in-phase (IP) loading can be seen from Fig. 4(f), where IP loading without mean stress/strain (path C) is compared to IP loading with a tensile mean stress/strain (path J) at the same effective strain amplitude. Figure 4(g) shows another example of the effect of mean stress on IP loading, by comparing the crack growth behavior for load path (F) with tensile mean stress and load path (G) with compressive mean stress. Again, presense of tensile mean stress accerelates the crack growth process. Figure 4(h) presents the effect of tensile mean normal stress/strain on out-of-phase loading, where OP loading without mean stress/strain (path N) is compared to OP loading with mean tensile stress/strain (path O). As can be seen, crack growth rate is higher for the OP loading with tensile mean stress/strain.

The effects of mean shear stress/strain on crack growth behavior and fatigue damage is shown in Fig. 4(i), where cyclic loading without mean shear stress/strain (path J) and with mean shear stress/strain (path F) are compared. As can be seen from this figure, crack growth rates are very similar under load paths J and F and, therefore, it may be concluded that mean shear stress/strain has no effect on crack growth and fatigue damage process as long as the maximum shear stress remains below yielding. The *FS* damage parameter only considers the effect of normal mean stress on fatigue damage process, consistent with these observations. The effect of normal mean stress is taken into account through the maximum normal stress term, $\sigma_{n,\max}$, which is composed of alternating and mean stress components.

CRACK GROWTH RATE CORRELATIONS

Cracking behavior and experimental observations as presented and discussed in the previous section suggest critical plane approaches are best suitable for fatigue life estimations under combined stresses. These approaches reflect the physical nature of fatigue damage process by considering specific plane(s) with maximum fatigue damage and are, therefore, also capable of predicting the crack path. As the cracks for all the

materials and loading conditions in this study were observed to be shear cracks, the *FS* critical plane parameter correctly represents the damage mechanism for these materials. The extension of this parameter for crack growth rate as proposed by Reddy and Fatemi (*RF*), presented by Eq. 1, was then used to correlate small crack growth rate data. This critical plane strain-based intensity factor, ΔK_{CPA}, considers the maximum shear strain amplitude as the main parameter driving the crack, and the normal stress on the maximum shear strain amplitude plane as the secondary parameter accelerating the crack growth rate if tensile, and retarding the crack growth rate if compressive.

Correlation of crack growth rate data for Inconel 718 based on *RF* critical plane intensity factor (Eq. 1 with $k = 1$) for the wide variety of load paths in Fig. 2 is shown in Fig. 6(a). As can be seen from this figure, Inconel 718 crack growth data are correlated reasonably well by the *RF* critical plane intensity factor, ΔK_{CPA}, for the multiaxial load paths including in-phase and out-of-phase tension-torsion with and without mean stresses. This critical plane intensity factor also correlates well crack growth rate data from biaxial tension-tension loading paths (paths U, V, and W in Fig. 2). Some of the data scatter in Fig. 6(a) can be explained by the interaction of crack networks observed, as coalescence or shielding of cracks can accelerate or retard the crack growth rate, respectively. Crack growth rate data correlations for IP and OP loading of 1050 N steel and Inconel 718 based on this critical plane intensity factor are presented in Fig. 6(b).

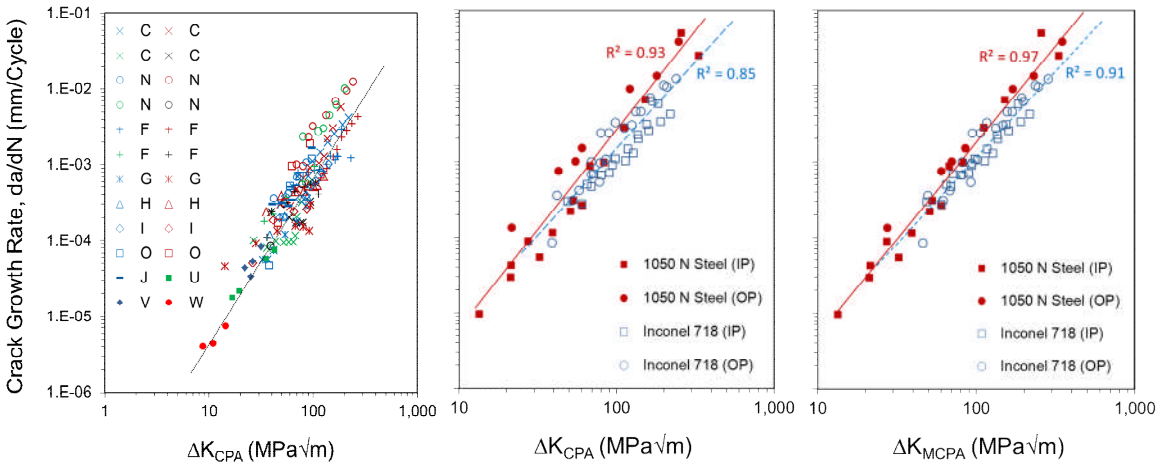

Figure 6. (a) Correlation of crack growth rates with Reddy-Fatemi critical plane strain intensity factor for Inconel 718 under various load paths. Correlation of IP (path C) and OP (path N) crack growth rate data for 1050 N steel and Inconel 718 with (b) Reddy-Fatemi critical plane strain intensity factor, and with (c) modified Reddy-Fatemi strain intensity factor considering the range of planes experiencing 95% of damage.

As presented earlier, micro-cracks were observed over a wider range of plane orientations around the critical plane for OP loading, as compared to IP loading. This

was explained by a wider range of planes experiencing a high percentage of damage value on the critical plane for OP loading, as presented in Fig. 5. A simple way of taking this effect into consideration is to modify the *RF* strain-based intensity factor as:

$$\Delta K_{MCPA} = G\,\Delta\gamma_{\max}\left(1+k\frac{\sigma_{n,\max}}{\sigma_y}\right)\sqrt{\frac{\Theta_{95,OP}}{\Theta_{95,IP}}\pi\,c} \tag{4}$$

where $\Theta_{95,IP}$ and $\Theta_{95,OP}$ are the range of plane orientation angles experiencing 95% of fatigue damage for IP and OP loading, respectively. The $\Theta_{95,IP}$ range for IP loading is typically about ±9º and the $\Theta_{95,OP}$ range for the example of OP loading shown in Fig. 5(b) is about ±17º. Therefore, this ratio is about 2. The correlation of crack growth rate data for IP and OP loading of 1050 N steel and Inconel 718 based on this modified version of the *RF* strain intensity factor is presented in Fig. 6(c). As can be seen form this figure, the correlation of IP and OP crack growth rate data is improved for both materials, as compared to the correlations in Fig. 6(b). Further data and more refined modeling may be needed to better capture this effect.

CONCLUSIONS

The following conclusions can be made based on the observed experimental results and analyses:

1) Cracks for all materials and loading conditions investigated in this study were found to be on or about the maximum shear plane. As the shear cracks typically have a zigzag pattern, surface roughness resulted in friction-induced closure. A compressive normal stress on the maximum shear plane was observed to decelerates crack growth and extend fatigue life, whereas a tensile normal stress accelerated crack growth and shortened fatigue life.
2) More cracks were observed for more ductile behaving materials, as compared to the more brittle behaving material. Shorter cracks were detected at earlier stage of the fatigue life for more ductile behaving materials. In addition, crack growth rate was higher for the more brittle behaving material.
3) Many more cracks in various sizes were observed for solid specimens, as compared to the tubular specimens, where cracks nucleated at smaller percentage of total fatigue life for the solid specimens. Crack growth rate was lower for the solid specimens, as compared to the tubular specimens, explained by the gradient of shear stress in the solid specimens.
4) More cracks were observed in higher amplitude tests, as compared to lower amplitude tests. Crack nucleation was also observed to occur at a much earlier stage of fatigue life for higher strain amplitude tests.
5) More cracks were observed for in-phase (IP) loading, as compared to 90º out-of-phase (OP) loading at the same strain level. Crack growth rate was higher for OP loading, which can be explained by a higher normal stress on the maximum shear

plane, compared to IP loading. Also, micro-cracks were observed over a wider range of plane orientations for OP loading, as compared to IP loading.

6) Presense of a tensile mean stress accerelates the crack growth process, resulting in an increased crack growth rate. A mean shear stress had no effect on crack growth and fatigue damage process, as long as the maximum shear stress was below yield strength.
7) Reddy-Fatemi effective strain-based intensity factor correlated crack growth rate data under combined stresses for all materials and the wide variety of load paths considered reasonably well. Crack growth rate correlations were improved by using a modified version of this parameter to account for the wider range of planes experiencing a high percentage of damage in OP loading, as compared to IP loading.

REFERENCES

1. Fatemi, A. and Shamsaei, N. (2011) *Int. J. Fatigue* **33**: 948-958.
2. Qian, J. and Fatemi, A. (1996) *Eng. Fract. Mech.* **55**: 969-990.
3. Bold, P.E., Brown, M.W., and Allen, R.J. (1992) *Fatigue Fract. Eng. Mater. Struct.* **15**: 965-977.
4. Guo, Y.H., Srivatsants, T.S., and Padovan, J. (1994) *Eng. Fract. Mech.* **47**: 843-866.
5. Erdogan, F. and Sih, G.C. (1963) *J. Bas. Eng., Trans. ASME* **85**: 519-525.
6. Sih, G.C. (1974) *Int. J. Fracture* **10**: 305-321.
7. Chen, X.M., Jiao, G.Q., and Cui, Z.Y. (1986) *Eng. Fract. Mech.* **24**: 127-144.
8. Zhang, H. and Fatemi, A. (2010) *Int. J. Fracture* **165**: 1-19.
9. Tanaka, K. (1974) *Eng. Fract. Mech.* **6**: 493-507.
10. Socie, D.F., Hua, C.T. and Worthem, D.W. (1987) *Fatigue Fract. Eng. Mater. Struct.* **10**: 1-16.
11. Reddy, S.C. and Fatemi, A. (1992). In: *Advances in Fatigue Lifetime Predictive Techniques*, pp. 569-585, Mitchell M.R. and Landgraf R.W. (Eds.), ASTM STP 1122, Philadelphia, PA.
12. Hoshide, T. and Socie, D.F. (1987) *Eng. Fract. Mech.* **26**: 841-850.
13. Shamsaei, N. and Fatemi, A. (2009) *Fatigue Fract. Eng. Mater. Struct.* **32**: 631-646.
14. ASTM Standard E2207-02 (2007) *Annual Book of ASTM Standards* **03.01**: 1297-1304.
15. Shamsaei, N., Fatemi, A., and Socie, D.F. (2011) *Int. J. Fatigue* **33**: 597-609.
16. Beer, T.A. (1984) Report UIUC-ENG 84-3606, University of Illinois at Urbana-Champaign, Illinois.
17. Fatemi, A. and Socie, D.F. (1988) *Fatigue Fract. Eng. Mater. Struct.* **11**: 149-165.
18. Shamsaei, N. (2010) PhD Dissertation, University of Toledo, Toledo, Ohio.
19. Shamsaei, N., Gladskyi, M., Panasovskyi, K., Shukaev, S., and Fatemi, A. (2010) *Int. J. Fatigue* **32**: 1862–1874.